WILEY *Journal of* MASS SPECTROMETRY

Mass spectrometry imaging of triglycerides in biological tissues by laser desorption ionization from silicon nanopost arrays

Jarod A. Fincher[1] | Andrew R. Korte[1] | Jacqueline E. Dyer[1] | Sridevi Yadavilli[2] | Nicholas J. Morris[3] | Derek R. Jones[4] | Victoria K. Shanmugam[4] | Russel K. Pirlo[5] | Akos Vertes[1] (iD)

[1] Department of Chemistry, The George Washington University, Washington, DC 20052, USA

[2] Research Center for Genetic Medicine, Children's National Medical Center, Washington, DC 20010, USA

[3] UES, Inc., Beavercreek, OH 45432, USA

[4] Division of Rheumatology, School of Medicine and Health Sciences, The George Washington University, Washington, DC 20037, USA

[5] Chemistry Division, U.S. Naval Research Laboratory, Washington, DC 20375, USA

Correspondence
Akos Vertes, Department of Chemistry, The George Washington University, Washington, DC 20052, USA.
Email: vertes@gwu.edu

Abstract

Mass spectrometry imaging (MSI) is used increasingly to simultaneously detect a broad range of biomolecules while mapping their spatial distributions within biological tissue sections. Matrix-assisted laser desorption ionization (MALDI) is recognized as the method-of-choice for MSI applications due in part to its broad molecular coverage. In spite of the remarkable advantages offered by MALDI, imaging of neutral lipids, such as triglycerides (TGs), from tissue has remained a significant challenge due to ion suppression of TGs by phospholipids, e.g. phosphatidylcholines (PCs). To help overcome this limitation, silicon nanopost array (NAPA) substrates were introduced to selectively ionize TGs from biological tissue sections. This matrix-free laser desorption ionization (LDI) platform was previously shown to provide enhanced ionization of certain lipid classes, such as hexosylceramides (HexCers) and phosphatidylethanolamines (PEs) from mouse brain tissue. In this work, we present NAPA as an MSI platform offering enhanced ionization efficiency for TGs from biological tissues relative to MALDI, allowing it to serve as a complement to MALDI-MSI. Analysis of a standard lipid mixture containing PC(18:1/18:1) and TG(16:0/16:0/16:0) by LDI from NAPA provided an ~49 and ~227-fold higher signal for TG(16:0/16:0/16:0) relative to MALDI, when analyzed without and with the addition of a sodium acetate, respectively. In contrast, MALDI provided an ~757 and ~295-fold higher signal for PC(18:1/18:1) compared with NAPA, without and with additional Na^+. Averaged signal intensities for TGs from MSI of mouse lung and human skin tissues exhibited an ~105 and ~49-fold increase, respectively, with LDI from NAPA compared with MALDI. With respect to PCs, MALDI provided an ~2 and ~19-fold increase in signal intensity for mouse lung and human skin tissues, respectively, when compared with NAPA. The complementary coverage obtained by the two platforms demonstrates the utility of using both techniques to maximize the information obtained from lipid MS or MSI experiments.

KEYWORDS

mass spectrometry imaging, laser desorption ionization, nanopost array, NAPA, lipids, triglycerides

1 | INTRODUCTION

Triglycerides (TGs) are an essential class of lipids found in most biological systems, where their primary function is energy storage. With regard to human health, TGs have been implicated in a host of potentially life-threatening diseases. For example, dyslipidemia, a condition characterized by elevated levels of TGs in plasma, has been linked to several major diseases such as metabolic syndrome, type-2 diabetes, coronary heart disease, and atherosclerosis.[1-4] Furthermore, TGs have also been linked to non-alcoholic fatty liver disease.[5] The prevalence and seriousness of these ailments has led to routine clinical testing for elevated levels of TGs. To better understand and treat these diseases, it is vital to develop analytical platforms capable of providing in-depth analysis of frequently difficult to detect neutral lipids in a complex matrix without isolation or separation.

Mass spectrometry imaging (MSI) is an analytical technique that allows for detection of a broad range of biomolecules, while simultaneously mapping their spatial distributions within a sample. Thus far, MSI platforms have been used to image biomolecules, including proteins, peptides, lipids, and small-molecule metabolites with great success.[6-10] The emergence of MSI can be attributed to the development of secondary ion mass spectrometry (SIMS) and matrix-assisted laser desorption ionization (MALDI), the first two MSI platforms to be used broadly.[11,12] Due to the low degree of fragmentation for organic molecules, and the large array of UV-absorbing matrices available, many with selectivity for certain biomolecular classes, MALDI is the current method-of-choice for MSI applications in biomedical studies.[13-15] Several matrix-free MSI platforms have been developed or adapted, including desorption electrospray ionization (DESI), desorption/ionization on silicon (DIOS), nanostructure-initiator mass spectrometry (NIMS), and laser ablation electrospray ionization (LAESI).[16-20]

Although remarkable success has been achieved by MALDI-MSI, significant challenges remain in the detection and analysis of neutral lipids, for example, TGs, from biological tissues.[21] This challenge arises due to suppression of TG ions by phosphatidylcholines (PCs), which constitute a majority of the lipid species present in mammalian cell membranes.[22,23] While the MALDI matrix 2,5-dihydroxybenzoic acid (DHB) is widely considered the gold standard for MS/MSI analysis of TGs, it has provided limited utility in ionizing TGs in MSI applications.[23-26] To overcome this limitation, several novel laser desorption ionization (LDI) methods employing silver or gold nanoparticles have been developed, resulting in significant enhancement in ion yields for TGs and a reduction in ion suppression by PCs.[27-29] While these alternative LDI methods have demonstrated impressive improvements in the detection of TGs, uniform deposition of the nanoparticles onto the tissue surface remains a challenge for successful MSI. Great care must be taken to avoid inhomogeneous matrix or nanoparticle deposition, which can lead to so-called "hot spots" and inaccurate spatial distributions for analytes.[30,31]

Silicon nanoposts arrays (NAPAs) are a highly uniform matrix-free LDI platform shown to provide ultra-trace sensitivity and broad molecular coverage.[32-34] Furthermore, MSI of biological tissues on NAPA indicated that detection of certain lipid classes, e.g., hexosylceramides (HexCers) and phosphatidylethanolamines (PEs), was enhanced compared to MALDI.[35,36] Here, we present NAPA as a matrix-free LDI-MSI platform offering enhanced ionization efficiency of neutral lipids, such as TGs, and demonstrate imaging applications for mouse lung and human skin tissue sections.

2 | EXPERIMENTAL

2.1 | Chemicals

The MALDI matrix 2,5-dihydroxybenzoic acid (DHB, catalog no. 58707) was purchased from Sigma-Aldrich (St. Louis, MO). LC-MS grade solvents water (catalog no. W6-212), chloroform (catalog no. C6704-4), methanol (catalog no. A452-4), acetonitrile (catalog no. A955-4), and sodium acetate (catalog no. S209-500) were all purchased from Fisher Scientific (Hampton, NH). Lipid standards 1,2,3-trihexadecanoyl-glycerol (TG[16:0/16:0/16:0] or TG[48:0], catalog no. 111000) and 1,2-dielaidoyl-sn-glycero-3-phosphocholine (PC[18:1/18:1] or PC[36:2], catalog no. 850376) were purchased from Avanti Polar Lipids, Inc. (Alabaster, AL).

2.2 | Fabrication of NAPA imaging chips

The nanofabrication process for NAPA chips for spot analysis and for imaging has been previously described.[36,37] Briefly, silicon nanoposts with final post dimensions of 1100 nm in height, 150 nm in diameter, and a periodicity of 337 nm were fabricated from high-conductivity p-type silicon wafers (Silicon Valley Microelectronics, Inc., Santa Clara, CA) using deep ultraviolet projection lithography (DUV-PL) followed by deep reactive ion etching (DRIE).

2.3 | Preparation of lipid standards

Lipid standards for TG(16:0/16:0/16:0) and PC(18:1/18:1) were dissolved and mixed to create a solution containing each compound at 1 mg/mL. For NAPA, lipid standards were prepared in chloroform and pipetted onto NAPA wells in 250 nL volumes. For MALDI, lipid standards were prepared in 73:18:9 isopropanol:methanol:water with a final concentration of 10 mg/mL DHB and pipetted in 500 nL volumes onto a stainless steel sample plate.

To assess the influence of salt addition on ionization efficiency of the lipid standard mixture, 250 nL of 100 μM sodium acetate was deposited onto NAPA wells and allowed to dry at atmospheric pressure before subsequent deposition of 250 nL aliquots of the lipid standard mixture. For MALDI, 100 μM sodium acetate was added to the sample solution prior to spotting. Analyses of the lipid standard mixture with and without salt were carried out in triplicates.

Given the different solvent compositions used for depositing the lipid standards mixture for MALDI and NAPA analysis, necessitated

by their different surface properties, microscope and chemical images were collected to ensure co-localization of the PC and TG lipid on NAPA substrates (see Figure S1 in the Supporting Information). For MALDI, the sample spots were uniform (i.e., they showed no prominent coffee ring effect), and the survey CPS function, which randomly samples pixels where matrix is present, was implemented for analysis.

2.4 | Tissue preparation for MSI

Human skin tissue samples were harvested from patients undergoing abdominoplasty and provided by The George Washington University School of Medicine and Health Sciences (Washington, DC) in accordance with protocols approved by the GW Institutional Review Board (GWU IRB 101419). Whole mouse lungs were provided by Children's National Medical Center (Washington, DC) in accordance with the protocol approved by the Institutional Animal Care and Use Committee (IACUC). All tissue samples were stored at -80 °C until analysis. A cryomicrotome (CM1800, Leica Microsystems Inc., Nussloch, Germany) operated at -25 °C was used to section 5 μm- and 10 μm-thick tissue sections for NAPA-LDI-MSI and MALDI-MSI experiments, respectively. Tissue sections were immediately thaw-mounted onto NAPA imaging chips or Superfrost Plus microscope slides (cat. no. 12-550-15, Fisher Scientific, Hampton, NH) for NAPA or MALDI analysis, respectively, and placed in a vacuum desiccator for 30 minutes before analysis. For MALDI-MSI experiments, matrix was applied using a Paasche airbrush TS-100D (Chicago, IL), with 10-15 cycles alternating between spraying 100 mg/mL DHB in 60% methanol for 10 s and a 30 s drying period.

2.5 | Imaging data acquisition and processing

All lipid standard and tissue imaging experiments were performed on a MALDI-LTQ-Orbitrap XL mass spectrometer (Thermo Scientific,

San Jose, CA) at a mass resolving power setting of 30,000. The instrument is equipped with a nitrogen laser emitting radiation at 337 nm with a 60 Hz repetition rate and a focal spot size of ~100 μm × 80 μm. Laser fluences ranging from 8 to 160 mJ/cm^2 were used for analysis of the lipid standard mixture, whereas fluences of 120 mJ/cm^2 and 150 mJ/cm^2 were used for all MALDI- and NAPA-MSI analyses, respectively. Experiments with standards used 3 laser shots/scan for NAPA and 10 shots/scan for MALDI. All MSI experiments used 3 shots/scan.

2.6 | Tissue extraction and UPLC-MS/MS

The complete tissue extraction protocol and UPLC-MS/MS conditions have been previously described.[35] Briefly, lipid extracts from intact mouse lung and human skin tissue samples were prepared and analyzed by data-dependent UPLC-MS/MS to help aid in the lipid assignments from MSI experiments. Tissue samples were homogenized using a hand-held homogenizer (TissueRuptor II, Qiagen, Hilden, Germany) in a 5 mL centrifuge tube containing 2 mL of 70% methanol (chilled to -80 °C). Following homogenization, an additional 2 mL of chloroform was added to induce phase separation and the chloroform layer was extracted and analyzed by UPLC-MS/MS. A Waters Acquity (Milford, MA) UPLC system, operated in reverse phase mode using a Waters Acquity UPLC CSH C18 column (2.1 mm × 100 mm × 1.7 μm) for chromatographic separation, was interfaced to an LTQ-Orbitrap XL mass spectrometer (Thermo Scientific, San Jose, CA).

3 | RESULTS AND DISCUSSION

Analysis of the nearly equimolar mixture of TG(16:0/16:0/16:0) and PC(18:1/18:1) by NAPA and MALDI demonstrated the ability of each platform to selectively ionize a particular lipid class (Figure 1).
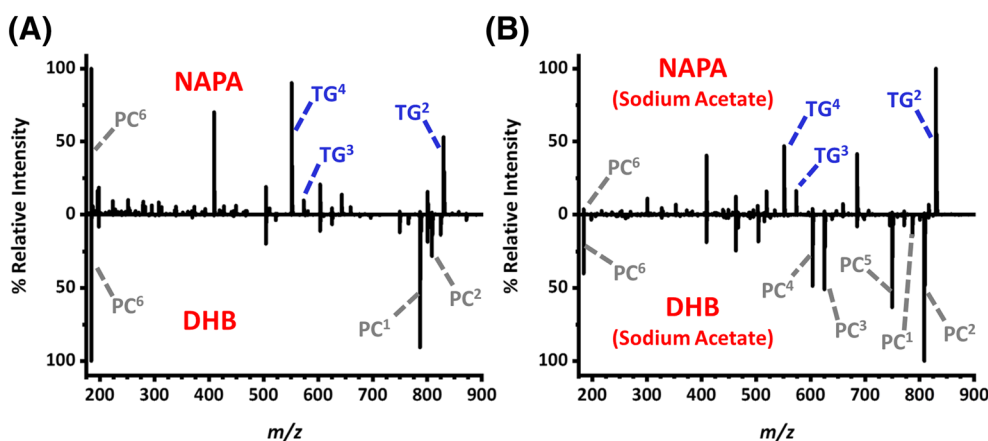

FIGURE 1 Mass spectra obtained by NAPA-LDI-MS and MALDI-MS analysis of a standard mixture containing TG(16:0/16:0/16:0) and PC(18:1/18:1) in positive ion mode a) without and b) with addition of sodium acetate. Ionic forms are denoted by superscripts: 1: [M+H]$^+$, 2: [M+Na]$^+$, 3: [M+Na-FA]$^+$, 4: [M+H-FA]$^+$, 5: [PC-Trimethylamine]$^+$, 6: [Phosphocholine+H]$^+$, and FA = fatty acid

NAPA demonstrated a high degree of selectivity for TG over PC, illustrated by a 49-fold higher signal intensity for that lipid relative to MALDI, which produced a marginal TG signal (Figure 1a). These findings are in agreement with previous MALDI studies demonstrating that PCs strongly suppress ionization of TGs.[22,23,38] The [TG +Na]+ adduct was the major TG-derived ion detected by NAPA, followed by diglyceride (DG)-like ions generated by in-source fragmentation. For NAPA substrates, significant in-source fragmentation of the PC lipid species was observed, as indicated by the strong peak at m/z 184.07, corresponding to the PC head group, phosphocholine (see Figure S2). In contrast, MALDI proved superior at ionizing the PC species with a 757-fold higher signal intensity for PC relative to NAPA (Figure 1a). For MALDI, the spectrum was dominated by the [PC+H]+ species, with lower detection of the [PC+Na]+ species.

To explore the role of alkali metals in ionization selectivity, sodium acetate was added to the lipid standard mixture before analysis by both NAPA and MALDI (Figure 1b). With added sodium acetate, NAPA provided a 227-fold higher signal intensity for TG relative to MALDI (see Table 1). This observation can be explained by both the increased availability of sodium ions, leading to a larger initial ion population, and to the increased stability of TG sodium adducts compared to protonated TGs, leading to significant

reduction in in-source fragmentation of TG ions into DG-like ions.[39-41] Interestingly, in the case of MALDI, the addition of sodium acetate led to a modest (4-fold) increase in TG signal (Table 1). Instead, the excess sodium cations available for potential adduction to TG shifted the ionization of PC from protonated to sodiated species. With sodium acetate, MALDI yielded a 295-fold higher signal intensity for PC relative to NAPA.

Analysis of the lipid standard mixture containing PC and TG at varied laser fluences showed that in the case of NAPA, increasing fluence led to increased TG signal and reduced PC signal (Figure 2a). At higher laser fluences (e.g., 80 mJ/cm2 and above), considerable melting of the nanoposts occurs, freeing up sodium cations for adduction to TG. Furthermore, at elevated laser fluences, PC appears to undergo significant in-source fragmentation when analyzed by NAPA (see Figure S2), resulting in the intact PC lipid being barely detected. This observation is in stark contrast to MALDI results, where the lipid signal composition remained unchanged across the fluence range examined. For all fluences, PC dominated the spectrum, indicating that ionization of TG by MALDI in the presence of PC is not fluence dependent. Similar experiments performed on lipid standards containing sodium acetate showed little to no fluence dependence for either NAPA or MALDI, with PC and TG dominating MALDI and NAPA spectra, respectively, at all tested fluences (Figure 2b). This finding supports the assumption that increased fluences in NAPA analysis liberate sodium for cationization.

To compare the ability of NAPA and MALDI to selectively ionize and image TGs and PCs from biological tissue, serial mouse lung tissue sections were analyzed. The PC and TG assignments based on accurate m/z from NAPA-LDI-MSI and MALDI-MSI and fragmentation data from UPLC-MS/MS analysis of tissue extracts are tabulated in Table S1. The integrated intensity of PC ions obtained by MALDI-MSI analysis of lung tissue was 2× higher than that obtained by NAPA (see Table 2). Conversely, NAPA provided an ~105-fold increase in integrated signal intensity for TGs relative to MALDI. Likewise, the number of detected PC species was higher with MALDI-MSI, whereas

TABLE 1 Relative intensities of TG(16:0/16:0/16:0) and PC(18:1/18:1) ions detected by NAPA-LDI-MS and MALDI-MS analysis of a binary mixture. Samples were analyzed without additive and with 100 μM sodium acetate. Values represent intensities summed for H+, Na+, and K+ adduct species and are scaled to the lowest intensity for the given lipid.

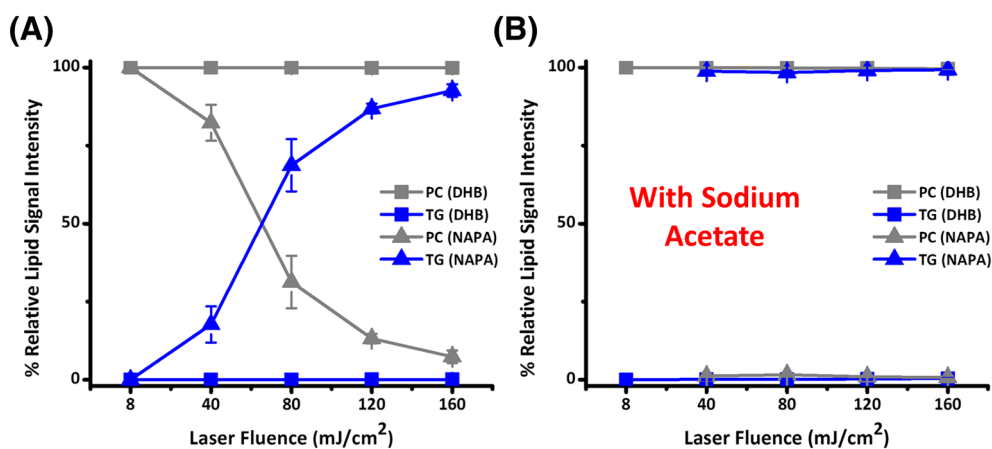| Lipid standard	Without sodium acetate		With sodium acetate	
	NAPA	**MALDI**	**NAPA**	**MALDI**
TG(48:0)	49	1	227	4
PC(36:2)	4	757	1	295

FIGURE 2 Relative lipid signal intensities as a function of laser fluence in NAPA-LDI-MS and MALDI-MS analysis of a standard mixture containing TG(16:0/16:0/16:0) and PC(18:1/18:1) in positive ion mode a) without and b) with addition of sodium acetate. No signal was detected at the lowest laser fluence (8 mJ/cm2) for NAPA-LDI-MS with addition of sodium acetate

TABLE 2 Relative intensities for PC and TG type ions, I_{PC} and I_{TG}, and total number of assigned species, n_{PC} and n_{TG}, from mouse lung and human skin tissue samples obtained by NAPA-LDI-MSI and MALDI-MSI. Intensities are scaled to the lowest intensity for the two techniques for each sample type. Lists of assigned PC and TG ions in mouse lung and human skin are available as Supplementary Information in Tables S1 and S2, respectively.

I and n	Mouse lung		Human skin	
	NAPA	MALDI	NAPA	MALDI
I_{PC}	1	2	1	19
n_{PC}	12	23	1	9
I_{TG}	105	1	49	1
n_{TG}	40	15	44	23

more TGs were present in the NAPA spectra (see Table 2). The effects of this complementarity on tissue imaging experiments are highlighted in Figure 3. The distributions of PC(36:4) and TG(52:3) are clearly

observed in the MALDI and NAPA datasets, respectively, but are weakly detected by the alternate technique. Individual (per image) normalization does reveal localized intensities for both lipids in both datasets (Figure S3) but due to the weak ion intensities, the distributions of the lower-intensity species (PC by NAPA and TG by MALDI) are not well defined.

Imaging of a diversity of compound classes was demonstrated on 10 um thick sections of mouse liver tissue. Distributions of additional TG species (TG(52:2) and TG(52:3)), and other compound classes (DG(32:0), PE(38:4), heme b, and taurocholic acid) were successfully acquired (see top panel in Figure S4). Comparing the NAPA-LDI and MALDI mass spectra gathered from these tissue sections, highlights the complementary nature of these techniques (see bottom panel in Figure S4).

To further explore the complementary coverage offered by NAPA-LDI-MSI and MALDI-MSI platforms across various sample types, serial human skin tissue sections were also imaged (see Figure 4). When comparing the overall coverage of PCs (Table 2),

FIGURE 3 Optical images (a and d) and chemical images (b, c, e, and f) of serial mouse lung tissue sections imaged by NAPA-LDI-MSI and MALDI-MSI platforms, respectively. Chemical images b) and e) represent the [M+H]$^+$ ionic species of PC(36:4), whereas c) and f) represent the [M+Na]$^+$ adduct of TG(52:3). Maximum image intensities are scaled equally between the two platforms to illustrate the differences in ionization efficiency of the respective lipids. Individually scaled images are available in Figure S2 of Supporting Information. g) Spectral comparison of MS scans averaged across entire tissue region
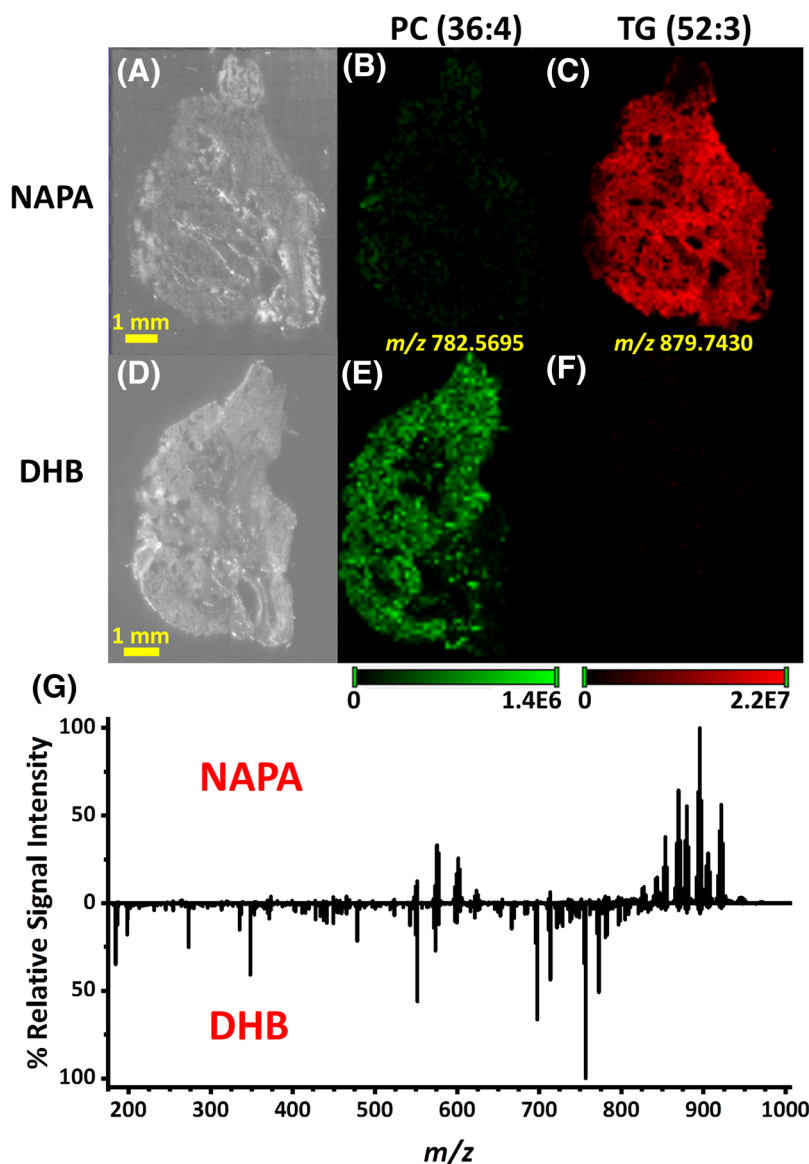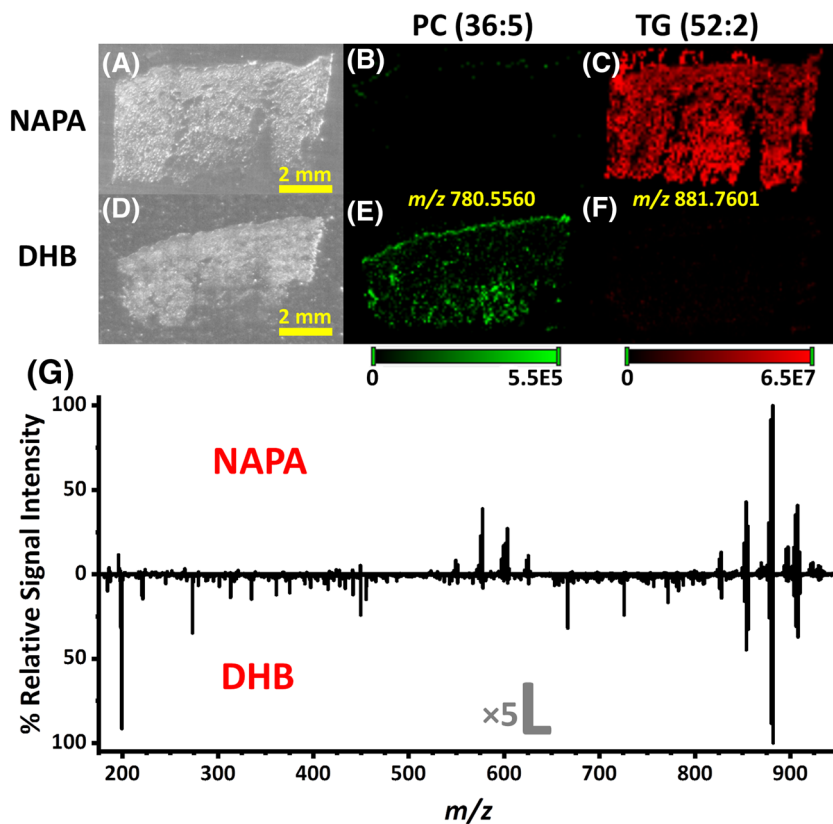
FIGURE 4 Optical images (a and d) and chemical images (b, c, e, and f) of serial human skin tissue sections imaged by NAPA-LDI-MSI and MALDI-MSI platforms, respectively. Chemical images b) and e) represent the [M+H]$^+$ ionic species of PC(36:5), whereas c) and f) represent the [M+Na]$^+$ adduct of TG(52:2). Maximum image intensities are scaled equally between the two platforms to illustrate the differences in ionization efficiency of the respective lipids. g) Spectral comparison of MS scans averaged across entire tissue region. Note that MALDI signal is amplified 5× above m/z 650

MALDI again outperformed NAPA by providing a 19× higher integrated signal intensity for PCs relative to NAPA. Conversely, NAPA demonstrated the ability to selectively ionize TGs by providing an ~49-fold increase in integrated signal intensity relative to MALDI. With regards to lipid distributions within the tissue, TG(52:2) was detected uniformly throughout the tissue by NAPA, whereas TG(52:2) was weakly detected throughout the tissue by MALDI. Conversely, MALDI detected PC(36:5) with relatively high sensitivity throughout the skin tissue as opposed to NAPA, where detection was sporadic.

4 | CONCLUSIONS

Analysis of a lipid standard mixture and MSI of different biological tissue types demonstrated that NAPA can serve as an MS/MSI platform providing enhanced ionization efficiency for TGs when compared to MALDI. In contrast, MALDI provided selectivity for PCs over TGs. The ability of NAPA-LDI-MSI to selectively ionize TGs while in the presence of PCs presents the possibility of using these two platforms in complementary MSI experiments to maximize molecular coverage for lipids. The use of MALDI to image certain lipid classes (e.g., PCs and sphingomyelins [SMs]) and NAPA to image other lipid classes (e.g., TGs, PEs, and HexCers) from serial sections promises to greatly expand the capabilities of MSI for studying the role of lipids in disease, infection, metabolism, and a host of other applications.

ORCID

Akos Vertes https://orcid.org/0000-0001-5186-5352

REFERENCES

1. Adiels M, Olofsson SO, Taskinen MR, Boren J. Overproduction of very-low-density lipoproteins is the hallmark of the dyslipidemia in the metabolic syndrome. *Arterioscler Thromb Vasc Biol*. 2008;28(7): 1225-1236.

2. Berenson GS, Srinivasan SR, Bao WH, Newman WP 3rd, Tracy RE, Wattigney WA. Association between multiple cardiovascular risk factors and atherosclerosis in children and young adults. *New Engl J Med*. 1998;338(23):1650-1656.

3. Ginsberg HN, Zhang YL, Hernandez-Ono A. Metabolic syndrome: Focus on dyslipidemia. *Obesity*. 2006;14(2S):41S-49S.

4. Taskinen MR. Diabetic dyslipidaemia: from basic research to clinical practice. *Diabetologia*. 2003;46(6):733-749.

5. Hamaguchi M, Kojima T, Takeda N, et al. The metabolic syndrome as a predictor of nonalcoholic fatty liver disease. *Ann Intern Med.* 2005;143(10):722-728.

6. Hutchinson RW, Cox AG, McLeod CW, et al. Imaging and spatial distribution of beta-amyloid peptide and metal ions in Alzheimer's plaques by laser ablation-inductively coupled plasma-mass spectrometry. *Anal Biochem.* 2005;346(2):225-233.

7. Jackson SN, Ugarov M, Egan T, et al. MALDI-ion mobility-TOFMS imaging of lipids in rat brain tissue. *J Mass Spectrom.* 2007;42(8):1093-1098.

8. Kertesz V, Van Berkel GJ, Vavrek M, Koeplinger KA, Schneider BB, Covey TR. Comparison of drug distribution images from whole-body thin tissue sections obtained using desorption electrospray ionization tandem mass spectrometry and autoradiography. *Anal Chem.* 2008;80(13):5168-5177.

9. Miura D, Fujimura Y, Yamato M, et al. Ultrahighly Sensitive in Situ Metabolomic Imaging for Visualizing Spatiotemporal Metabolic Behaviors. *Anal Chem.* 2010;82(23):9789-9796.

10. Seeley EH, Oppenheimer SR, Mi D, Chaurand P, Caprioli RM. Enhancement of protein sensitivity for MALDI imaging mass spectrometry after chemical treatment of tissue sections. *J Am Soc Mass Spectrom.* 2008;19(8):1069-1077.

11. Caprioli RM, Farmer TB, Gile J. Molecular imaging of biological samples: Localization of peptides and proteins using MALDI-TOF MS. *Anal Chem.* 1997;69(23):4751-4760.

12. Sjovall P, Lausmaa J, Johansson B. Mass spectrometric imaging of lipids in brain tissue. *Anal Chem.* 2004;76(15):4271-4278.

13. Buchberger AR, DeLaney K, Johnson J, Li LJ. Mass Spectrometry Imaging: A Review of Emerging Advancements and Future Insights. *Anal Chem.* 2018;90(1):240-265.

14. Fitzgerald MC, Parr GR, Smith LM. Basic matrices for the matrix-assisted laser desorption/ionization mass spectrometry of proteins and oligonucleotides. *Anal Chem.* 1993;65(22):3204-3211.

15. Thomas A, Charbonneau JL, Fournaise E, Chaurand P. Sublimation of New Matrix Candidates for High Spatial Resolution Imaging Mass Spectrometry of Lipids: Enhanced Information in Both Positive and Negative Polarities after 1,5-Diaminonapthalene Deposition. *Anal Chem.* 2012;84(4):2048-2054.

16. Nemes P, Vertes A. Laser ablation electrospray ionization for atmospheric pressure, in vivo, and imaging mass spectrometry. *Anal Chem.* 2007;79(21):8098-8106.

17. Northen TR, Yanes O, Northen MT, et al. Clathrate nanostructures for mass spectrometry. *Nature.* 2007;449(7165):1033-U1033.

18. Shen ZX, Thomas JJ, Averbuj C, et al. Porous silicon as a versatile platform for laser desorption/ionization mass spectrometry. *Anal Chem.* 2001;73(3):612-619.

19. Takats Z, Wiseman JM, Gologan B, Cooks RG. Mass spectrometry sampling under ambient conditions with desorption electrospray ionization. *Science.* 2004;306(5695):471-473.

20. Wei J, Buriak JM, Siuzdak G. Desorption-ionization mass spectrometry on porous silicon. *Nature.* 1999;399(6733):243-246.

21. Murphy RC. Challenges in mass spectrometry-based lipidomics of neutral lipids. *Trac-Trends in Analytical Chemistry.* 2018;107:91-98.

22. Emerson B, Gidden J, Lay JO Jr, Durham B. A rapid separation technique for overcoming suppression of triacylglycerols by phosphatidylcholine using MALDI-TOF MS. *J Lipid Res.* 2010;51(8):2428-2434.

23. Asbury GR, Al-Saad K, Siems WF, Hannan RM, Hill HH. Analysis of triacylglycerols and whole oils by matrix-assisted laser desorption/ionization time of flight mass spectrometry. *J Am Soc Mass Spectrom.* 1999;10(10):983-991.

24. Hayasaka T, Goto-Inoue N, Zaima N, Kimura Y, Setou M. Organ-Specific Distributions of Lysophosphatidylcholine and Triacylglycerol in Mouse Embryo. *Lipids.* 2009;44(9):837-848.

25. Horn PJ, Silva JE, Anderson D, et al. Imaging heterogeneity of membrane and storage lipids in transgenic Camelina sativa seeds with altered fatty acid profiles. *Plant J.* 2013;76(1):138-150.

26. Nishikawa K, Hashimoto M, Itoh Y, et al. Detection of changes in the structure and distribution map of triacylglycerol in fatty liver model by MALDI-SpiralTOF. *Febs Open Bio.* 2014;4:179-184.

27. Dufresne M, Masson JF, Chaurand P. Sodium-Doped Gold-Assisted Laser Desorption Ionization for Enhanced Imaging Mass Spectrometry of Triacylglycerols from Thin Tissue Sections. *Anal Chem.* 2016;88(11):6018-6025.

28. Jackson SN, Baldwin K, Muller L, et al. Imaging of lipids in rat heart by MALDI-MS with silver nanoparticles. *Anal Bioanal Chem.* 2014;406(5):1377-1386.

29. Son J, Lee G, Cha S. Direct Analysis of Triacylglycerols from Crude Lipid Mixtures by Gold Nanoparticle-Assisted Laser Desorption/Ionization Mass Spectrometry. *J Am Soc Mass Spectrom.* 2014;25(5):891-894.

30. Alexandrov T. MALDI imaging mass spectrometry: statistical data analysis and current computational challenges. *BMC Bioinformatics.* 2012;13(S16):S11.

31. Goodwin RJA. Sample preparation for mass spectrometry imaging: Small mistakes can lead to big consequences. *J Proteomics.* 2012;75(16):4893-4911.

32. Korte AR, Stopka SA, Morris N, Razunguzwa T, Vertes A. Large-Scale Metabolite Analysis of Standards and Human Serum by Laser Desorption Ionization Mass Spectrometry from Silicon Nanopost Arrays. *Anal Chem.* 2016;88(18):8989-8996.

33. Walker BN, Stolee JA, Pickel DL, Retterer ST, Vertes A. Tailored Silicon Nanopost Arrays for Resonant Nanophotonic Ion Production. *J Phys Chem C.* 2010;114(11):4835-4840.

34. Walker BN, Stolee JA, Vertes A. Nanophotonic Ionization for Ultratrace and Single-Cell Analysis by Mass Spectrometry. *Anal Chem.* 2012;84(18):7756-7762.

35. Fincher JA, Dyer JE, Korte AR, Yadavilli S, Morris NJ, Vertes A. Matrix-free mass spectrometry imaging of mouse brain tissue sections on silicon nanopost arrays. *J Comp Neurol.* 2018;527(13):2101-2121.

36. Stopka SA, Rong C, Korte AR, et al. Molecular Imaging of Biological Samples on Nanophotonic Laser Desorption Ionization Platforms. *Angew Chem Int Ed.* 2016;55(14):4482-4486.

37. Morris NJ, Anderson H, Thibeault B, Vertes A, Powell MJ, Razunguzwa TT. Laser desorption ionization (LDI) silicon nanopost array chips fabricated using deep UV projection lithography and deep reactive ion etching. *RSC Adv.* 2015;5(88):72051-72057.

38. Petkovic M, Schiller J, Muller M, et al. Detection of individual phospholipids in lipid mixtures by matrix-assisted laser desorption/ionization time-of-flight mass spectrometry: Phosphatidylcholine prevents the detection of further species. *Anal Biochem.* 2001;289(2):202-216.

39. Herrera LC, Potvin MA, Melanson JE. Quantitative analysis of positional isomers of triacylglycerols via electrospray ionization tandem mass spectrometry of sodiated adducts. *Rapid Commun Mass Spectrom.* 2010;24(18):2745-2752.

40. Picariello G, Paduano A, Sacchi R, Addeo F. MALDI-TOF Mass Spectrometry Profiling of Polar and Nonpolar Fractions in Heated Vegetable Oils. *J Agric Food Chem.* 2009;57(12):5391-5400.

41. Pittenauer E, Allmaier G. The Renaissance of High-Energy CID for Structural Elucidation of Complex Lipids: MALDI-TOF/RTOF-MS of

Alkali Cationized Triacylglycerols. *J Am Soc Mass Spectrom.* 2009;20(6):1037-1047.

SUPPORTING INFORMATION

Additional supporting information may be found online in the Supporting Information section at the end of the article.

Supporting Information

for

Mass Spectrometry Imaging of Triglycerides in Biological Tissues by Laser Desorption Ionization from Silicon Nanopost Arrays

Jarod A. Fincher,[1] Andrew R. Korte,[1] Jacqueline E. Dyer,[1] Sridevi Yadavilli,[2] Nicholas J. Morris,[3] Derek R. Jones,[4] Victoria K. Shanmugam,[4] Russel K. Pirlo,[5] and Akos Vertes*[1]

1Department of Chemistry, The George Washington University, Washington, DC 20052, USA

2Research Center for Genetic Medicine, Children's National Medical Center, Washington, DC 20010, USA

3UES, Inc., Beavercreek, OH 45432, USA

4Division of Rheumatology, The George Washington University, School of Medicine and Health Sciences, Washington, DC 20037, USA

5Chemistry Division, U.S. Naval Research Laboratory, Washington, DC 20375, USA

*Correspondence: Akos Vertes, Department of Chemistry, The George Washington University, Washington, DC 20052, USA.

Email: vertes@gwu.edu
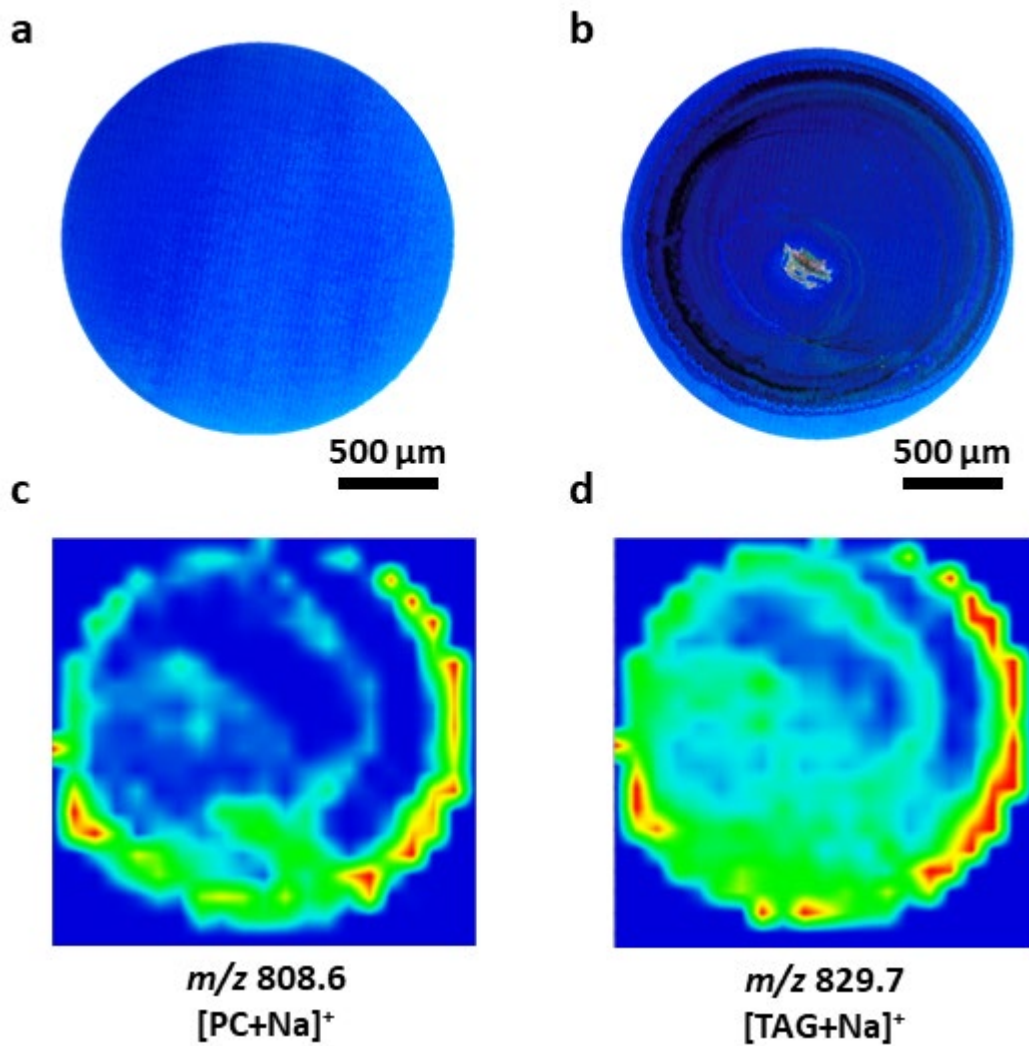
Figure S1 Optical images (a and b) of sodium acetate and sodium acetate plus lipid standards mixture deposited onto NAPA, respectively. Chemical images (c and d) of sodiated PC(36:2) detected at *m/z* 808.6 and TG(48:0) detected at *m/z* 829.7, illustrating the co-localization of the deposited lipid species.
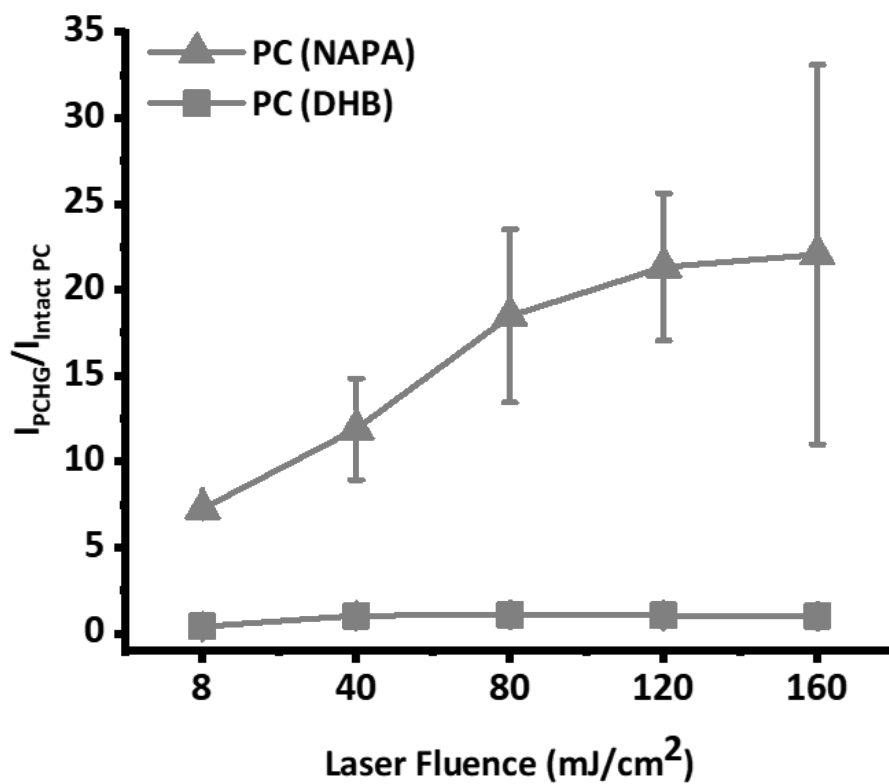
Figure S2 Ratio of ion intensities for phosphocholine headgroup fragment, I_{PCHG}, to summed intact PC lipid adducts, $I_{Intact\,PC}$, as a function of laser fluence for a lipid standard PC(18:1/18:1) analyzed by MALDI-MS and NAPA-LDI-MS.
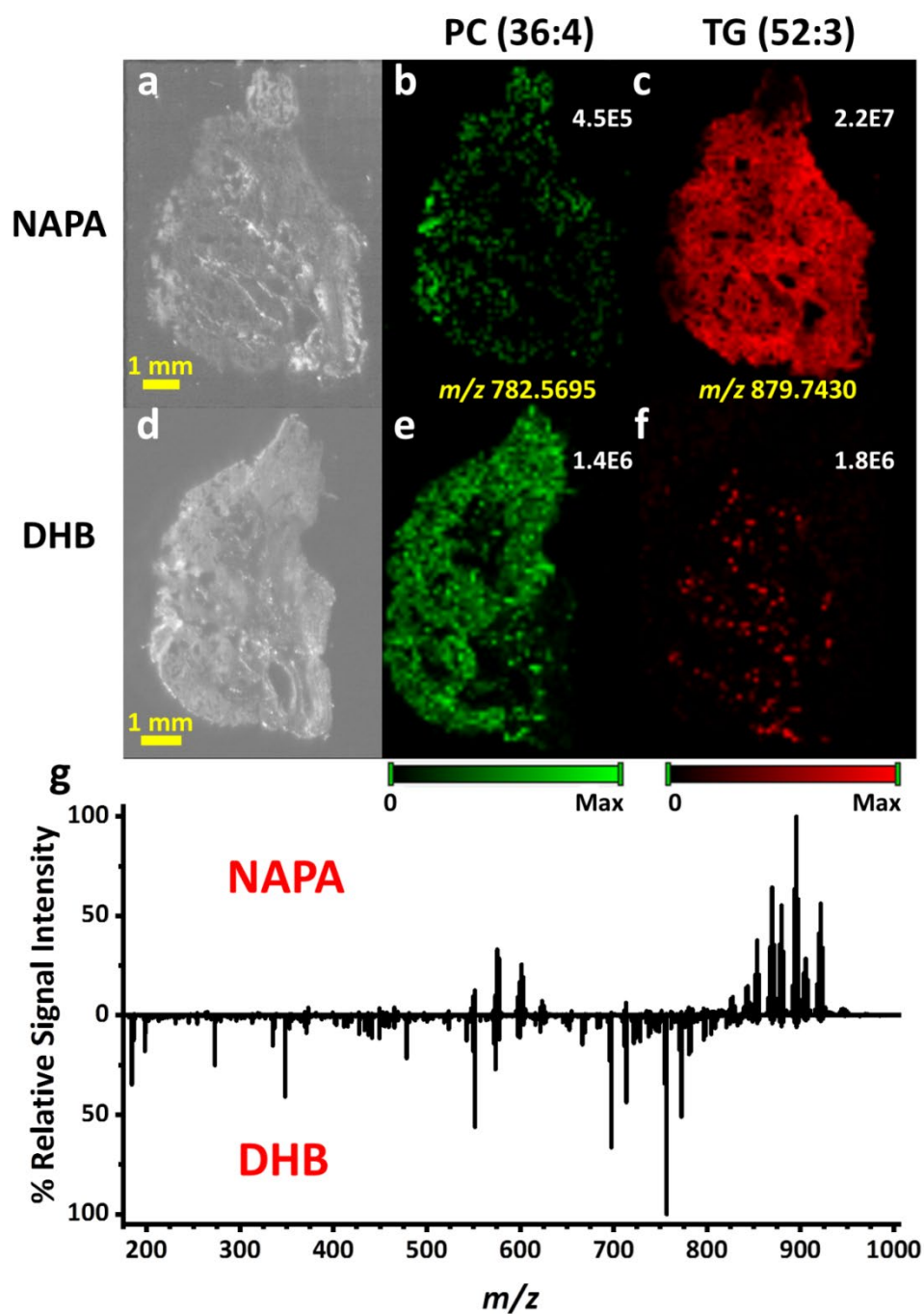
Figure S3 Optical images (a and d) and chemical images (b, c, e, and f) of serial mouse lung tissue sections imaged by NAPA-LDI-MSI and MALDI-MSI platforms, respectively. Chemical images b) and e) represent the [M+H]+ ionic species of PC(36:4), whereas c) and f) represent the [M+Na]+ adduct of TG(52:3). Individual images were not scaled equally (maximum image intensity in arbitrary units is found in top right corner of respective image) between the two platforms to illustrate the differences in ionization efficiency for the respective lipids. g) Spectral comparison of MS scans averaged across the entire tissue region.
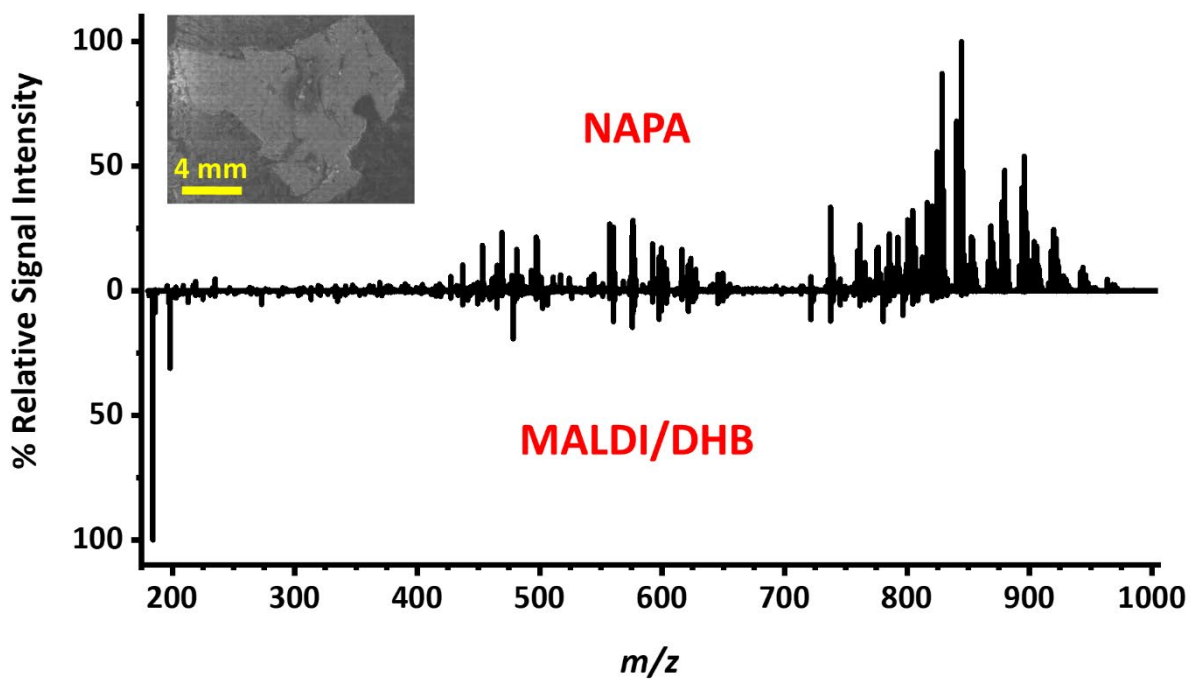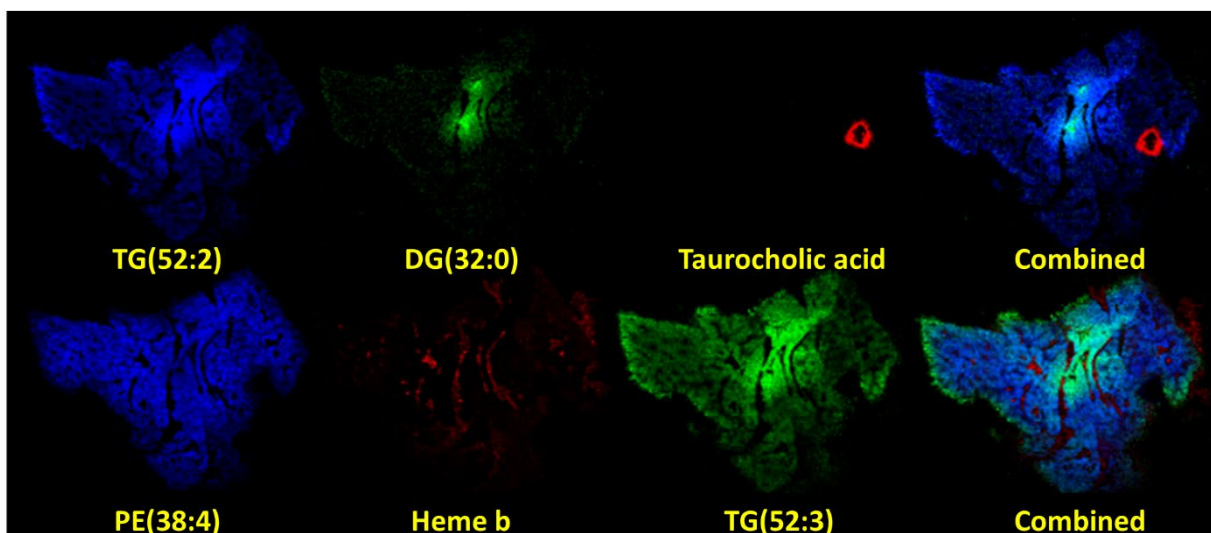
Figure S4 Top panel shows chemical images for diverse compound classes by NAPA-LDI-MSI from 10 μm thick sections of mouse liver tissue. Comparing the NAPA-LDI and MALDI mass spectra gathered from these tissue sections (see Bottom panel) highlights the complementary nature of these techniques.

Table S1 PC and TG lipid identifications from NAPA-LDI-MSI, MALDI-MSI, and UPLC-MS/MS analysis of mouse lung tissue.

Lipid ID	Fatty Acids from LC-MS/MS	Chemical Formula	Ionic Species	Calc. m/z	Δ ppm (NAPA)	Δ ppm (MALDI)
PC(30:0)	14:0, 16:0	$C_{38}H_{76}NO_8P$	$[M+H]^+$	706.5381	x	0.7
			$[M+K]^+$	744.4940	-2.0	0.4
			$[M+Na]^+$	728.5201	x	0.1
PC(32:1)	14:0, 18:1, 16:0, 16:1	$C_{40}H_{78}NO_8P$	$[M+2K-H]^+$	808.4656	-1.1	x
			$[M+H]^+$	732.5538	x	0.3
			$[M+K]^+$	770.5097	-0.8	-0.1
			$[M+Na]^+$	754.5357	-0.5	0.2
			$[M+Na+K-H]^+$	792.4916	-0.1	x
PC(32:2)	14:0, 18:2, 16:1	$C_{40}H_{76}NO_8P$	$[M+K]^+$	768.4940	-4.0	x
			$[M+Na]^+$	752.5201	x	1.6
PC(32:3)		$C_{40}H_{74}NO_8P$	$[M+H]^+$	728.5225	x	-3.2
PC(34:0)	16:0, 18:0	$C_{42}H_{84}NO_8P$	$[M+2K-H]^+$	838.5125	-0.1	x
PC(34:1)	16:0, 18:1	$C_{42}H_{82}NO_8P$	$[M+2K-H]^+$	836.4969	-0.9	x
			$[M+H]^+$	760.5851	x	0.4
			$[M+K]^+$	798.5410	0.8	1.1
			$[M+Na]^+$	782.5670	x	0.6
PC(34:2)		$C_{42}H_{80}NO_8P$	$[M+2K-H]^+$	834.4812	0.2	x
			$[M+K]^+$	796.5253	-2.0	-0.1
			$[M-H_2O+H]^+$	740.5589	x	-4.0
PC(34:3)	16:0, 18:3, 16:1, 18:2	$C_{42}H_{78}NO_8P$	$[M+H]^+$	756.5538	-3.5	-3.0
			$[M+K]^+$	794.5097	-3.2	x
			$[M+Na]^+$	778.5357	x	-1.7
PC(34:4)	14:0, 20:4	$C_{42}H_{76}NO_8P$	$[M+H]^+$	754.5381	-3.7	-3.0
			$[M+K]^+$	792.4940	-3.1	x
PC(34:5)		$C_{42}H_{74}NO_8P$	$[M+H]^+$	752.5225	x	-1.6
PC(36:1)	18:0, 18:1	$C_{44}H_{86}NO_8P$	$[M+K]^+$	826.5723	x	1.1
PC(36:2)	16:0, 20:2, 18:0, 18:2, 18:1	$C_{44}H_{84}NO_8P$	$[M+H]^+$	786.6007	x	0.8
			$[M+K]^+$	824.5566	-1.0	0.5
			$[M+Na]^+$	808.5827	x	0.5
PC(36:4)	16:0, 20:4, 18:2	$C_{44}H_{80}NO_8P$	$[M+H]^+$	782.5694	1.3	-2.5
			$[M+K]^+$	820.5253	-1.0	-0.1
PC(36:5)	16:0, 20:5, 16:1, 20:4	$C_{44}H_{78}NO_8P$	$[M+H]^+$	780.5538	x	-3.2
PC(36:7)		$C_{44}H_{74}NO_8P$	$[M-H_2O+H]^+$	758.5119	-2.3	-1.7
PC(38:4)	16:0, 22:4, 18:1, 20:3	$C_{46}H_{84}NO_8P$	$[M+H]^+$	810.6007	x	-1.9
			$[M+K]^+$	848.5566	x	0.4
			$[M+Na]^+$	832.5827	x	0.7

PC(38:5)	16:0, 22:5, 18:0, 20:5, 18:1, 20:4	C$_{46}$H$_{82}$NO$_8$P	[M+K]$^+$	846.5410	x	0.8
			[M+Na]$^+$	830.5670	x	0.8
PC(38:6)	16:0, 22:6, 18:2, 20:4	C$_{46}$H$_{80}$NO$_8$P	[M+H]$^+$	806.5694	x	-1.8
			[M+K]$^+$	844.5253	x	-0.2
			[M+Na]$^+$	828.5514	x	0.1
PC(38:7)		C$_{46}$H$_{78}$NO$_8$P	[M+H]$^+$	804.5538	x	-2.5
PC(38:8)		C$_{46}$H$_{76}$NO$_8$P	[M-H$_2$0+H]$^+$	784.5276	x	-1.7
PC(40:6)	18:0, 22:6	C$_{48}$H$_{84}$NO$_8$P	[M+K]$^+$	872.5566	x	-2.3
			[M+Na]$^+$	856.5827	x	0.4
TG(42:0)		C$_{45}$H$_{86}$O$_6$	[M+2Na-H]$^+$	767.6136	3.2	x
TG(42:1)		C$_{45}$H$_{84}$O$_6$	[M+2Na-H]$^+$	765.5980	3.3	x
TG(42:2)		C$_{45}$H$_{82}$O$_6$	[M+Na]$^+$	741.6004	0.1	x
TG(44:0)		C$_{47}$H$_{90}$O$_6$	[M+2Na-H]$^+$	795.6449	3.1	x
TG(44:1)	14:0, 16:1, 14:1, 18:1, 12:0, 16:0, 10:0, 16:0	C$_{47}$H$_{88}$O$_6$	[M+2Na-H]$^+$	793.6293	3.3	x
TG(44:2)	12:0, 14:0, 18:2, 10:0, 16:0	C$_{47}$H$_{86}$O$_6$	[M+K]$^+$	785.6056	0.9	x
			[M+Na]$^+$	769.6317	-0.2	x
TG(44:3)		C$_{47}$H$_{84}$O$_6$	[M+Na]$^+$	767.6160	0.1	x
TG(44:4)		C$_{47}$H$_{82}$O$_6$	[M+Na]$^+$	765.6004	0.1	x
TG(46:0)		C$_{49}$H$_{94}$O$_6$	[M+K]$^+$	817.6682	0.1	x
			[M+Na]$^+$	801.6943	-0.2	x
TG(46:1)	14:0, 18:1, 16:0, 16:1, 14:1, 12:0	C$_{49}$H$_{92}$O$_6$	[M+2Na-H]$^+$	821.6606	3.2	x
			[M+K]$^+$	815.6526	0.8	x
			[M+Na]$^+$	799.6786	0.0	x
			[M+Na+K-H]$^+$	837.6345	3.8	x
TG(46:2)	14:0, 18:2, 12:0, 16:1, 14:1, 16:0, 10:0, 18:1	C$_{49}$H$_{90}$O$_6$	[M+K]$^+$	813.6369	0.8	x
			[M+Na]$^+$	797.6630	-0.1	x
TG(46:3)	14:0, 18:3, 14:1, 18:2, 12:0, 16:0, 10:0, 18:1, 16:1	C$_{49}$H$_{88}$O$_6$	[M+K]$^+$	811.6213	1.6	x
			[M+Na]$^+$	795.6473	0.1	x
TG(48:0)		C$_{51}$H$_{98}$O$_6$	[M+K]$^+$	845.6995	1.1	1.5
			[M+Na]$^+$	829.7256	-0.3	-0.3
TG(48:1)	16:0, 16:1, 18:0, 14:0, 18:1	C$_{51}$H$_{96}$O$_6$	[M+K]$^+$	843.6839	1.3	1.4

			[M+Na]$^+$	827.7099	0.1	-0.2
TG(48:2)	14:0, 16:0, 18:2, 16:1, 18:1, 14:1	C$_{51}$H$_{94}$O$_6$	[M+K]$^+$	841.6682	0.8	1.0
			[M+Na]$^+$	825.6943	0.5	0.4
TG(48:3)	14:0, 16:1, 18:2, 14:1, 16:0, 12:0, 18:1	C$_{51}$H$_{92}$O$_6$	[M+K]$^+$	839.6526	0.9	x
			[M+Na]$^+$	823.6786	0.6	x
TG(50:1)	16:0, 18:1	C$_{53}$H$_{100}$O$_6$	[M+K]$^+$	871.7152	0.7	1.2
			[M+Na]$^+$	855.7412	-0.4	-0.3
TG(50:2)	16:0, 16:1, 18:1	C$_{53}$H$_{98}$O$_6$	[M+K]$^+$	869.6995	1.1	1.1
			[M+Na]$^+$	853.7256	0.4	0.3
TG(50:3)	16:0, 16:1, 18:2, 14:0, 18:1	C$_{53}$H$_{96}$O$_6$	[M+K]$^+$	867.6839	0.9	0.9
			[M+Na]$^+$	851.7099	0.6	0.5
TG(50:4)	14:0, 18:2, 16:1, 14:1, 18:1	C$_{53}$H$_{94}$O$_6$	[M+K]$^+$	865.6682	0.8	0.2
			[M+Na]$^+$	849.6943	0.6	0.2
TG(50:5)		C$_{53}$H$_{92}$O$_6$	[M+K]$^+$	863.6526	1.4	x
TG(52:2)	16:0, 18:1	C$_{55}$H$_{102}$O$_6$	[M+K]$^+$	897.7308	-0.7	0.6
			[M+Na]$^+$	881.7569	-1.2	-0.5
TG(52:3)	16:0, 18:1, 18:2	C$_{55}$H$_{100}$O$_6$	[M+K]$^+$	895.7152	0.0	0.8
			[M+Na]$^+$	879.7412	0.0	0.4
TG(52:4)	16:0, 18:2, 16:1, 18:1	C$_{55}$H$_{98}$O$_6$	[M+K]$^+$	893.6995	0.3	0.4
			[M+Na]$^+$	877.7256	0.4	0.4
TG(52:5)	16:1, 18:2, 18:1, 18:3	C$_{55}$H$_{96}$O$_6$	[M+K]$^+$	891.6839	0.4	-0.4
			[M+Na]$^+$	875.7099	0.6	-0.3
TG(52:6)	16:1, 18:2, 18:3	C$_{55}$H$_{94}$O$_6$	[M+K]$^+$	889.6682	0.6	x
TG(54:3)	18:0, 18:1, 18:2, 16:0, 20:1	C$_{57}$H$_{104}$O$_6$	[M+K]$^+$	923.7465	-1.2	0.4
			[M+Na]$^+$	907.7725	-1.6	-0.5
TG(54:4)	18:0, 18:2, 18:1	C$_{57}$H$_{102}$O$_6$	[M+K]$^+$	921.7308	-0.7	0.6
			[M+Na]$^+$	905.7569	-0.9	0.0
TG(54:5)	18:1, 18:2, 16:0, 22:5, 20:3, 20:4, 18:3	C$_{57}$H$_{100}$O$_6$	[M+K]$^+$	919.7152	-0.4	0.1
			[M+Na]$^+$	903.7412	-0.4	0.2
TG(54:6)	18:2, 18:1, 18:3, 16:1, 20:3	C$_{57}$H$_{98}$O$_6$	[M+K]$^+$	917.6995	-0.1	-0.5
			[M+Na]$^+$	901.7256	-0.8	-0.7
TG(54:7)	18:2, 18:3, 18:1	C$_{57}$H$_{96}$O$_6$	[M+K]$^+$	915.6839	-0.4	x
TG(56:3)		C$_{59}$H$_{108}$O$_6$	[M+K]$^+$	951.7778	-2.7	x
			[M+Na]$^+$	935.8038	-2.3	x

TG(56:4)	18:1, 18:1, 20:2	$C_{59}H_{106}O_6$	[M+2Na-H]$^+$	955.7701	1.4	x
			[M+K]$^+$	949.7621	-0.7	x
			[M+Na]$^+$	933.7882	-1.0	x
			[M+Na+K-H]$^+$	971.7441	2.8	x
TG(56:5)		$C_{59}H_{104}O_6$	[M+K]$^+$	947.7465	0.1	x
			[M+Na]$^+$	931.7725	-0.8	x
TG(56:6)		$C_{59}H_{102}O_6$	[M+K]$^+$	945.7308	0.0	x
			[M+Na]$^+$	929.7569	-1.3	x
TG(56:7)		$C_{59}H_{100}O_6$	[M+K]$^+$	943.7152	0.2	x
TG(56:8)		$C_{59}H_{98}O_6$	[M+K]$^+$	941.6995	-0.2	x
TG(58:8)		$C_{61}H_{102}O_6$	[M+K]$^+$	969.7308	0.4	x
TG(60:13)		$C_{63}H_{96}O_6$	[M-H$_2$0+H]$^+$	931.7174	0.3	x

Table S2 PC and TG lipid identifications from analysis of human skin tissue.

Lipid ID	Fatty Acids from LC-MS/MS	Chemical Formula	Ionic Species	Calc. m/z	Δ ppm (NAPA)	Δ ppm (MALDI)
PC(38:4)	16:0, 22:4, 18:1, 20:3	$C_{46}H_{84}NO_8P$	$[M+H]^+$	810.6007	x	-3.1
PC(36:5)	16:0, 20:5, 16:1, 20:4	$C_{44}H_{78}NO_8P$	$[M+H]^+$	780.5538	-2.6	-2.9
PC(34:3)	16:0, 18:3, 16:1, 18:2	$C_{42}H_{78}NO_8P$	$[M+H]^+$	756.5538	x	-2.7
PC(36:4)	16:0, 20:4, 18:2	$C_{44}H_{80}NO_8P$	$[M+H]^+$	782.5694	x	-2.5
TG(54:2)	18:0, 18:2, 16:0, 20:0, 16:0, 18:1, 20:1	$C_{57}H_{106}O_6$	$[M+Na]^+$	909.7882	-4.2	-2.4
PC(38:7)		$C_{46}H_{78}NO_8P$	$[M+H]^+$	804.5538	x	-2.4
PC(38:6)	16:0, 22:6, 18:2, 20:4	$C_{46}H_{80}NO_8P$	$[M+H]^+$	806.5694	x	-2.0
PC(34:2)		$C_{42}H_{80}NO_8P$	$[M+K]^+$	796.5253	-3.0	-1.5
TG(52:4)	16:0, 18:2, 16:1, 18:1	$C_{55}H_{98}O_6$	$[M+K]^+$	893.6995	-0.2	-1.2
PC(36:2)	16:0, 20:2, 18:0, 18:2, 18:1	$C_{44}H_{84}NO_8P$	$[M+H]^+$	786.6007	x	-1.1
TG(56:4)	18:1, 20:2	$C_{59}H_{106}O_6$	$[M+Na]^+$	933.7882	-2.5	-0.9
TG(50:3)	16:0, 16:1, 18:2, 14:0, 18:1	$C_{53}H_{96}O_6$	$[M+K]^+$	867.6839	0.8	-0.8
PC(34:1)	16:0, 18:1	$C_{42}H_{82}NO_8P$	$[M+H]^+$	760.5851	x	-0.8
TG(46:1)	14:0, 18:1, 16:0, 16:1, 14:1, 12:0	$C_{49}H_{92}O_6$	$[M+Na]^+$	799.6786	-0.4	-0.3
PC(34:2)		$C_{42}H_{80}NO_8P$	$[M+H]^+$	758.5694	x	-0.2
TG(52:2)	16:0, 18:1	$C_{55}H_{102}O_6$	$[M+Na]^+$	881.7569	-1.1	-0.2
TG(56:5)		$C_{59}H_{104}O_6$	$[M+Na]^+$	931.7725	-1.3	-0.1
TG(54:3)	18:0, 18:1, 18:2, 16:0, 20:1	$C_{57}H_{104}O_6$	$[M+Na]^+$	907.7725	-1.2	0.0
TG(48:3)	14:0, 16:1, 18:2, 14:1, 16:0, 12:0, 18:1	$C_{51}H_{92}O_6$	$[M+Na]^+$	823.6786	0.2	0.1
TG(50:1)	16:0, 18:1	$C_{53}H_{100}O_6$	$[M+Na]^+$	855.7412	-0.4	0.1
TG(56:3)		$C_{59}H_{108}O_6$	$[M+Na]^+$	935.8038	-1.4	0.2
PC(34:1)	16:0, 18:1	$C_{42}H_{82}NO_8P$	$[M+K]^+$	798.541	x	0.4
TG(52:3)	16:0, 18:1, 18:2	$C_{55}H_{100}O_6$	$[M+Na]^+$	879.7412	0.1	0.5
TG(54:3)	18:0, 18:1, 18:2, 16:0, 20:1,	$C_{57}H_{104}O_6$	$[M+K]^+$	923.7465	-0.7	0.6
TG(54:6)	18:2, 18:1, 18:3, 16:1, 20:3	$C_{57}H_{98}O_6$	$[M+Na]^+$	901.7256	-1.2	0.6

TG(54:4)	18:0, 18:2, 18:1	$C_{57}H_{102}O_6$	[M+Na]$^+$	905.7569	-0.9	0.6
TG(48:2)	14:0, 16:0, 18:2, 16:1, 14:0, 18:1, 14:1	$C_{51}H_{94}O_6$	[M+Na]$^+$	825.6943	0.2	0.6
PC(34:1)	16:0, 18:1	$C_{42}H_{82}NO_8P$	[M+Na]$^+$	782.567	x	0.6
TG(50:2)	16:0, 16:1, 18:1	$C_{53}H_{98}O_6$	[M+Na]$^+$	853.7256	0.1	0.7
TG(52:5)	16:1, 18:2, 18:1, 18:3	$C_{55}H_{96}O_6$	[M+Na]$^+$	875.7099	0.8	0.7
TG(56:7)		$C_{59}H_{100}O_6$	[M+Na]$^+$	927.7412	-1.6	0.7
PC(36:2)	16:0, 20:2, 18:0, 18:2, 18:1	$C_{44}H_{84}NO_8P$	[M+Na]$^+$	808.5827	x	0.7
PC(38:4)	16:0, 22:4, 18:1, 20:3	$C_{46}H_{84}NO_8P$	[M+Na]$^+$	832.5827	x	0.8
TG(54:5)	18:1, 18:2, 16:0, 22:5, 20:3, 20:4, 18:3	$C_{57}H_{100}O_6$	[M+Na]$^+$	903.7412	-0.6	0.8
TG(56:6)		$C_{59}H_{102}O_6$	[M+Na]$^+$	929.7569	-1.0	0.8
TG(48:1)	16:0, 16:1, 14:0, 18:0, 14:0, 18:1	$C_{51}H_{96}O_6$	[M+Na]$^+$	827.7099	-0.2	0.8
TG(50:3)	16:0, 16:1, 18:2, 14:0, 18:1	$C_{53}H_{96}O_6$	[M+Na]$^+$	851.7099	0.5	0.8
TG(52:4)	16:0, 18:2, 16:1, 18:1	$C_{55}H_{98}O_6$	[M+Na]$^+$	877.7256	0.5	0.9
TG(52:3)	16:0, 18:1, 18:2	$C_{55}H_{100}O_6$	[M+K]$^+$	895.7152	-0.2	0.9
TG(50:4)	14:0, 18:2, 16:1, 14:1, 18:1	$C_{53}H_{94}O_6$	[M+Na]$^+$	849.6943	0.5	1.1
TG(52:2)	16:0, 18:1	$C_{55}H_{102}O_6$	[M+K]$^+$	897.7308	-0.4	1.2
TG(50:2)	16:0, 16:1, 18:1	$C_{53}H_{98}O_6$	[M+K]$^+$	869.6995	1.3	1.3
PC(36:2)	16:0, 20:2, 18:0, 18:2, 18:1	$C_{44}H_{84}NO_8P$	[M+K]$^+$	824.5566	x	1.3
TG(46:0)		$C_{49}H_{94}O_6$	[M+Na]$^+$	801.6943	-0.1	1.3
TG(48:1)	16:0, 16:1, 14:0, 18:0, 18:1	$C_{51}H_{96}O_6$	[M+K]$^+$	843.6839	1.0	1.8
TG(50:1)	16:0, 18:1	$C_{53}H_{100}O_6$	[M+K]$^+$	871.7152	1.2	2.0
TG(54:2)	18:0, 18:2, 16:0, 20:0, 18:1, 16:0, 20:1	$C_{57}H_{106}O_6$	[M+K]$^+$	925.7621	-3.5	x
TG(42:1)		$C_{45}H_{84}O_6$	[M+Na]$^+$	743.616	-2.5	x
TG(60:10)		$C_{63}H_{102}O_6$	[M-H$_2$O+H]$^+$	937.7644	-1.8	x
TG(56:4)	18:1, 20:2	$C_{59}H_{106}O_6$	[M+K]$^+$	949.7621	-1.7	x

TG(46:2)	14:0, 18:2, 12:0, 16:0, 16:1, 14:1, 18:1, 10:0	$C_{49}H_{90}O_6$	[M+Na]$^+$	797.663	-0.8	x
TG(44:3)		$C_{47}H_{84}O_6$	[M+Na]$^+$	767.616	-0.7	x
TG(58:6)		$C_{61}H_{106}O_6$	[M+Na]$^+$	957.7882	-0.7	x
TG(42:2)		$C_{45}H_{82}O_6$	[M+Na]$^+$	741.6004	-0.7	x
TG(54:5)	18:1, 18:2, 16:0, 22:5, 20:3, 20:4, 18:3	$C_{57}H_{100}O_6$	[M+K]$^+$	919.7152	-0.7	x
TG(44:2)	12:0, 14:0, 18:2, 10:0, 16:0	$C_{47}H_{86}O_6$	[M+Na]$^+$	769.6317	-0.6	x
TG(54:4)	18:0, 18:2, 18:1	$C_{57}H_{102}O_6$	[M+K]$^+$	921.7308	-0.6	x
TG(44:0)		$C_{47}H_{90}O_6$	[M+Na]$^+$	773.663	-0.6	x
TG(56:8)		$C_{59}H_{98}O_6$	[M+K]$^+$	941.6995	-0.6	x
TG(54:7)	18:2, 18:3, 18:1	$C_{57}H_{96}O_6$	[M+K]$^+$	915.6839	-0.5	x
TG(54:6)	18:2, 18:1, 18:3, 16:1, 20:3	$C_{57}H_{98}O_6$	[M+K]$^+$	917.6995	-0.4	x
TG(44:4)		$C_{47}H_{82}O_6$	[M+Na]$^+$	765.6004	-0.4	x
TG(52:6)	16:1, 18:2, 18:3	$C_{55}H_{94}O_6$	[M+K]$^+$	889.6682	-0.3	x
TG(46:5)		$C_{49}H_{84}O_6$	[M+Na]$^+$	791.616	-0.3	x
TG(46:3)	14:0, 18:3, 14:1, 18:2, 16:1, 12:0, 16:0, 10:0, 18:1	$C_{49}H_{88}O_6$	[M+Na]$^+$	795.6473	-0.2	x
TG(52:5)	16:1, 18:2, 18:1, 18:3	$C_{55}H_{96}O_6$	[M+K]$^+$	891.6839	-0.2	x
TG(56:5)		$C_{59}H_{104}O_6$	[M+K]$^+$	947.7465	-0.1	x
TG(56:7)		$C_{59}H_{100}O_6$	[M+K]$^+$	943.7152	-0.1	x
TG(50:5)		$C_{53}H_{92}O_6$	[M+Na]$^+$	847.6786	0.1	x
TG(46:0)		$C_{49}H_{94}O_6$	[M+K]$^+$	817.6682	0.1	x
TG(56:6)		$C_{59}H_{102}O_6$	[M+K]$^+$	945.7308	0.1	x
TG(58:6)		$C_{61}H_{106}O_6$	[M+K]$^+$	973.7621	0.2	x
TG(48:5)		$C_{51}H_{88}O_6$	[M+Na]$^+$	819.6473	0.5	x
TG(60:11)		$C_{63}H_{100}O_6$	[M-H$_2$O+H]$^+$	935.7487	0.5	x
TG(48:2)	14:0, 16:0, 18:2, 16:1, 18:1, 14:1	$C_{51}H_{94}O_6$	[M+K]$^+$	841.6682	0.5	x
TG(58:8)		$C_{61}H_{102}O_6$	[M+K]$^+$	969.7308	0.6	x

TG(46:1)	14:0, 16:0, 16:1, 14:1, 12:0, 18:1	$C_{49}H_{92}O_6$	$[M+K]^+$	815.6526	0.8	x
TG(50:4)	14:0, 18:2, 16:1, 14:1, 18:1	$C_{53}H_{94}O_6$	$[M+K]^+$	865.6682	0.8	x
TG(46:2)	14:0, 18:2, 12:0, 16:0, 16:1, 14:1, 18:1, 10:0	$C_{49}H_{90}O_6$	$[M+K]^+$	813.6369	1.0	x
TG(48:3)	14:0, 16:1, 18:2, 14:1, 16:0, 12:0, 18:1	$C_{51}H_{92}O_6$	$[M+K]^+$	839.6526	1.0	x
TG(50:5)		$C_{53}H_{92}O_6$	$[M+K]^+$	863.6526	1.3	x
TG(58:8)		$C_{61}H_{102}O_6$	$[M+Na]^+$	953.7569	1.4	x
TG(46:3)	14:0, 18:3, 14:1, 18:2, 18:2, 12:0, 16:0, 10:0, 18:1, , 16:1	$C_{49}H_{88}O_6$	$[M+K]^+$	811.6213	1.7	x
TG(56:4)	18:1, 20:2	$C_{59}H_{106}O_6$	$[M+2Na-H]^+$	955.7701	2.3	x
TG(40:1)		$C_{43}H_{80}O_6$	$[M+2Na-H]^+$	737.5667	2.4	x
TG(42:0)		$C_{45}H_{86}O_6$	$[M+2Na-H]^+$	767.6136	2.4	x
TG(44:2)	12:0, 14:0, 18:2, 10:0, 16:0, 18:2	$C_{47}H_{86}O_6$	$[M+2Na-H]^+$	791.6136	2.8	x
TG(42:1)		$C_{45}H_{84}O_6$	$[M+2Na-H]^+$	765.598	2.8	x
TG(44:0)		$C_{47}H_{90}O_6$	$[M+2Na-H]^+$	795.6449	2.8	x
TG(56:4)	18:1, 20:2	$C_{59}H_{106}O_6$	$[M+Na+K-H]^+$	971.7441	2.8	x
TG(44:1)	14:0, 16:1, 14:1, 16:0, 12:0, 18:1, 12:0, 10:0, 18:1	$C_{47}H_{88}O_6$	$[M+2Na-H]^+$	793.6293	2.9	x
TG(46:1)	14:0, 18:1, 16:0, 16:1, 14:1, 12:0	$C_{49}H_{92}O_6$	$[M+2Na-H]^+$	821.6606	3.1	x